Journal of Chemical Technology and Metallurgy, 54, 4, 2019, 715-720

CHARACTERISTICS OF $LaCrO_3$ NANOMATERIAL
THE EFFECT OF THE CALCINATION TEMPERATURE

Rudy Situmeang[1] , Simon Sembiring[2], Wasinton Simanjuntak[1],

Zipora Sembiring[1], Suripto Dwi Yuwono[1]

[1] *Department of Chemistry, University of Lampung*
Bandar Lampung 35145, Indonesia
[2] *Department of Physics, University of Lampung*
Bandar Lampung 35145, Indonesia
E-mail: rudy.tahan@fmipa.unila.ac.id

Received 15 March 2018
Accepted 22 February 2019

ABSTRACT

$LaCrO_3$ nanomaterial is prepared using simultaneously the sol–gel and the freeze-drying method. Nitrate salts of lanthanum and chrome are dissolved in a pectin solution. The sample is thoroughly stirred using a magnetic stirrer while adjusting pH to 11 until a gel is formed. After the freeze-drying process, the precursors are subjected to a calcination treatment at 600°C, 700°C, and 800°C and subsequently characterized by X-ray diffraction (XRD), TEM and DRS analyses. The results verify that a major crystalline phase of $LaCrO_3$ perovskite is formed as the temperature of calcination increases. The crystallites size identification using the Scherrer equation shows that the size increases with calcination temperature increase. But the grain size analysis by TEM verifies that the calcination temperature has in fact a small effect on the size. The DRS analysis indicates that the band-gap energy is affected by the calcination temperature. The values obtained increase from 2.62 eV to 2.89 eV and 2.98 eV with temperature increase.

Keywords: nano, perovskite, band-gap energy, sol-gel, freeze-drying.

INTRODUCTION

The perovskite compound is one of the fascinating materials which is widely used in industrial applications, such as photovoltaic solar cell [1, 2], optical coatings [3, 4], ceramics [5, 6], magnetic materials [7, 8], sensors [9, 10], and catalysts [11, 12] . It exhibits a peculiar physical and chemical characteristics such as conductivity, ion mobility through a crystal lattice, a thermal and chemical stability, as well as acid and base sites, magnetic, electrocatalytic and photocatalytic properties.

In principle, the perovskite material of the general formula of ABO_3 can be synthesized by mixing the salt or the oxide of rare earth or third main group elements with the salt or the oxide of transition elements. The larger cations fit into the A sites, while the smaller cations fit into the B sites of the crystalline structure. The simple ABO_3 composition follows the limits of the tolerance factor, $t = 0.71(r_A+r_o)/(r_B+r_o)$ [13 - 15]. This t-value refers to the formation of cubic, orthorhombic, and hexagonal crystalline structures. The choice of the preparation methods such as the sol-gel one [16, 17], the coprecipitation [18, 19], the hydrothermal [20, 21] and auto-combustion [22, 23] plays an important role in determining the characteristics of the perovskite materials of importance for their application. Even though so many methods of preparation have been claimed to give an excellent result [24, 25], the sol-gel method offers some advantages such as a homogenous product of a large surface area, a control of its stoichiometric composition, and nanosize particles formation [26, 27].

This study reports the effect of the calcination temperature on the characteristics of the nano sized $LaCrO_3$ which is prepared by the sol-gel method. It emphasizes the importance of a calcination in absence of a hydrogen flow.

EXPERIMENTAL

Materials and Instruments

$La(NO_3)_3.6H_2O$, NH_3, and $Cr(NO_3)_3.9H_2O$ were reagent grade chemicals obtained from Merck. Pectin as an emulsifying agent was purchased from the local market, while the distilled water was produced in our laboratory. The characteristics of the perovskite sample were studied by X-ray Diffraction, XRD (Philips-PW 1710), Transmission Electron Microscopy, TEM (JEOL, JEM-1400), and Diffuse Reflectance Spectrophotometry, DRS (Shimadzu 2450). A Nabertherm electrical furnace (Lilienthal, Germany) was used for samples calcination.

Procedure

The solid $LaCrO_3$ was prepared by dissolving a specified mass of $La(NO_3)_3.9H_2O$, and $Cr(NO_3)_3.6H_2O$, respectively, in 100 mL of 4 % pectin solution. The mixture was stirred until a homogenous solution was obtained and then freeze-dried. The dry samples were calcined to 600°C, 700°C, and 800°C, respectively, using a temperature program with a temperature increase of 2°C min^{-1}. Upon reaching the final temperature value the calcination proceeded within 2 h in absence of a hydrogen flow. This procedure was different from the one previously used [28].

Characterization

To compare the characteristics of $LaCrO_3$ obtained by using both the sol-gel and the freeze-drying methods, the samples were characterized by several techniques. The structure and the crystalline phase formed were identified by X-ray diffraction analysis. The instrument used Cu K_α radiation (l = 1.5418 Å) produced at 40 kV and 30 mA with a step size of 0.02. The surface morphology and the microstructure were identified by TEM. The analysis was conducted on polished and thermally etched samples with different magnifications [29]. The band-gap energy of the sample was analyzed by a diffuse reflectance spectrophotometer.

RESULTS AND DISCUSSION

X-Ray Diffraction Analysis

The XRD patterns of the samples calcined at 600ºC, 700ºC and 800ºC are collected and treated qualitatively by comparing the diffraction peaks with those of the standard Powder Diffraction Data Base of JCPD files. The investigation shows that $LaCrO_3$ perovskite is the major phase [30]. The fullprof program of the Rietveld method is applied to study the effect of the calcination temperature on the phase composition and the unit cell parameters. The Rietveld plot is depicted in Fig.1 below. It is evident that the diffractograms, in principle, are practically similar, with a difference in the intensity, the position, and hkl plane of the highest intensity.

The vertical line (green) corresponds to the hkl plane. The blue line refers to the difference between the observed and the calculated data. Fig. 1 shows that the difference between the observed and the calculated data is quite small. Hence, the Rietveld refinement leads to an excellent agreement. The overall Rietveld refinement results

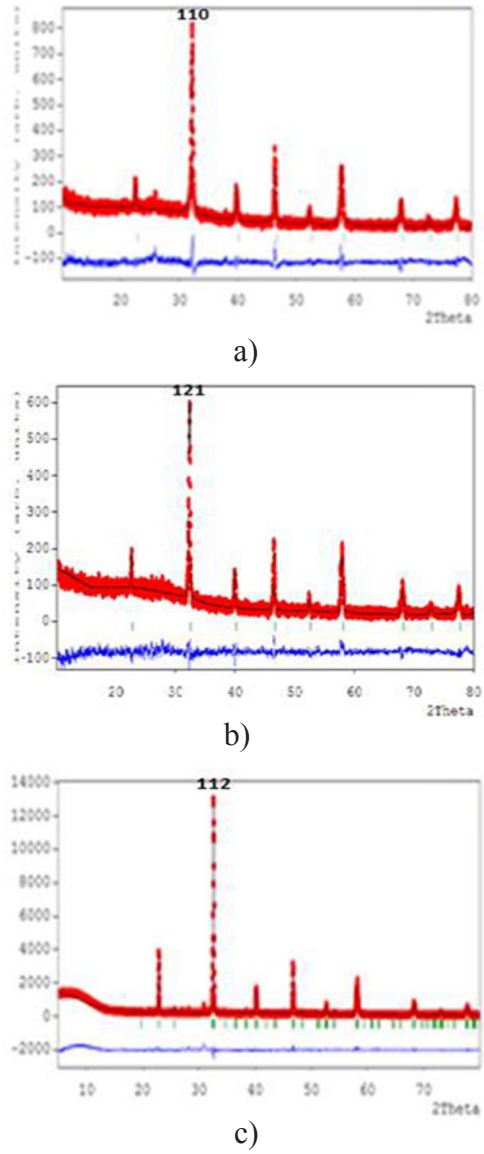

Fig. 1. XRD Rietveld plots of $LaCrO_3$ calcined at: (a) 600°C; (b) 700°C; and (c) 800°C. The experimental data is shown by a solid line, while the calculated one - by the red-dot line.

Table 1. Rietveld refinement referring to $LaCrO_3$ as a function of the calcination temperature (600°C, 700°C, and 800°C).

$LaCrO_3$ calcined at	hkl	JCPD File	χ^2	a (Å)	b (Å)	c (Å)	V (Å^3)
600°C	110	44-0333	1.5	3.8842	3.8842	3.8842	58.6096
700°C	121	33-0701	1.7	5.4788	7.7575	5.5148	234.3888
800°C	112	24-1016	2.1	5.5162	5.4805	7.7522	234.3609

referring to $LaCrO_3$ are listed in Table 1. Table 1 shows that (χ^2) values of all $LaCrO_3$ samples are relatively low, which is in correspondence with the basic principle of acceptance $\chi^2 \leq 4$ [31]. Perovskite $LaCrO_3$ is the main phase observed at all calcination temperatures studied. However, the crystalline structure is quite different. It is cubic in case of 600°C calcination with Miller index of the most intense diffraction peak of 110 according to PDF 44-0333. The structure transforms with increrase of the calcination temperature. The Miller index of the most intense diffraction peak of the samples calcined at 700°C and 800°C refers to 121 and 112, respectively. As a consequence, the volume of the unit cell increases also.

Transmission Electron Analysis

The characterization of the samples using TEM is illustrated in Fig. 2. It is evident that particles agglomeration proceeds. However, the existence of a crystalline structure as a unit cell is still identified. As shown in Fig. 3(a), the shape of the crystal is cubic at a certain position (red-arrow). Fig. 3(b) shows that the shape of $LaCrO_3$ is orthorhombhohedral (red arrow) and hexagonal (green arrow) at certain sites. According to Fig.3(c), the crystal is rhombhohedral (red arrow) and hexagonal (green arrow). The crystallites size is usually below 50 nm. Thus, $LaCrO_3$ can be considered a nano material.

Diffuse Reflectance Spectroscopy Analysis

The diffuse reflectance spectrophotometry is a common technique in determining the band- gap energy of a powder sample [32]. The Kubelka – Munk method [33] is used in this study. It is based on the equation:

$$\alpha(h\nu) \approx \beta\,(h\nu - E_{op})^n \qquad (1)$$

where β is a constant, n is an index of values of 1/2, 3/2, 2 or 3 depending on the nature of the electron transition responsible for the absorption. Values of 1/2 or 3/2

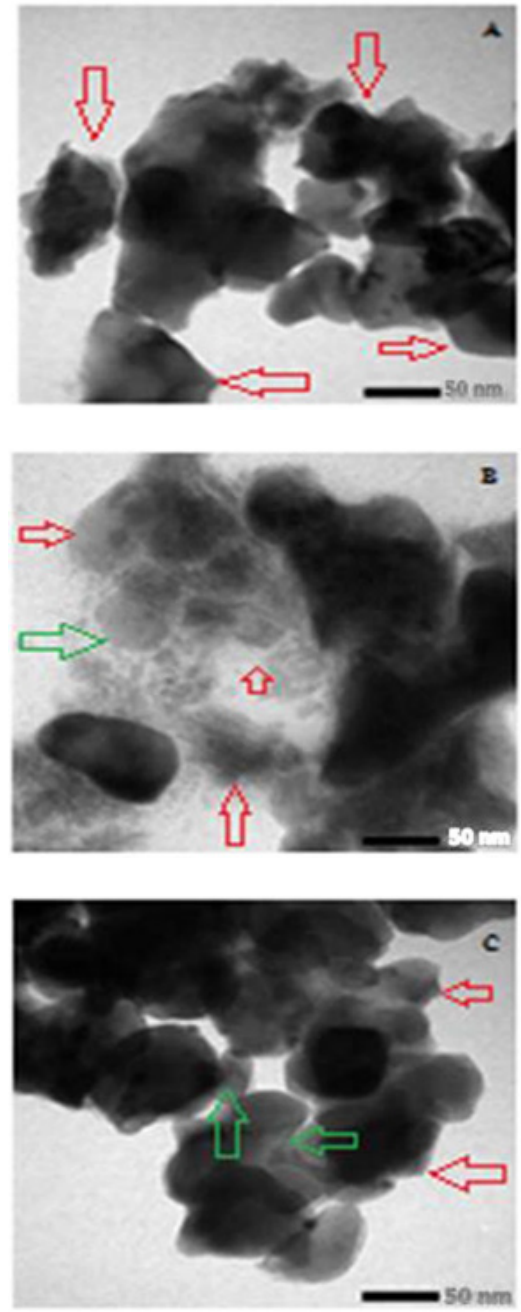

Fig. 2. Micrographs of $LaCrO_3$ calcined at: (A) 600°C; (B) 700°C; (C) 800°C.

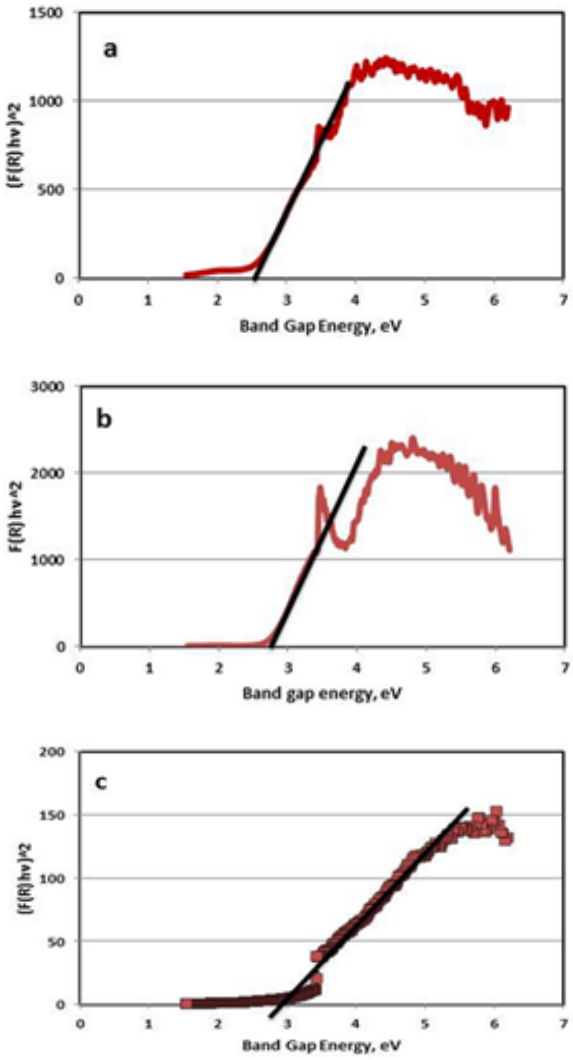

Fig. 3. Band Gap Energy of $LaCrO_3$ calcined at 600°C (a), 700°C (b), and 800°C (c).

referring to a direct transition are allowed or forbidden in a quantum mechanical sense, while those of 2 or 3 correspond to an allowed or a forbidden indirect transition, respectively [34]. The relation between $(\alpha\ h\nu)^2$ versus $(h\nu)$ plot according to Eq. (1) is shown in Fig. 3. The direct optical gap energy can be obtained from the intercept of the resulting straight lines with the energy axis at $(\alpha\ h\nu)^2 = 0$.

The band-gap energy of $LaCrO_3$ prepared at 600°C, 700°C and 800°C is 2.62 eV, 2.89 eV, and 2.98 eV, respectively. This result implies that the increase of the calcination temperature widens the band energy gap of $LaCrO_3$. Furthermore, the value referring to 800°C is in an agreement with that of a previous investigation [35].

CONCLUSIONS

The present investigation demonstrates the effect of the calcination temperature on $LaCrO_3$ characteristics. The XRD results reveal that the crystalline phase formation is influenced by the calcination temperature applied. The unit cell parameter elongation corresponds to the calcination temperature increase. As a consequence, the volume of the unit cell increases. The morphology of the samples identified by TEM is characterized by the existence of particles of a various size and shape. It can be implied that $LaCrO_3$ nanomaterial is formed whose particles size is less than 50 nm. Furthermore, the band-gap energy is also affected by the temperature of calcination. Its value increases with calcination temperature increase.

Acknowledgements

The authors are grateful to the Research Institution of The Directorate General of Higher Education of Republic of Indonesia (KEMENRISTEKDIKTI) for the funding provided through the Decentralization Research Grant (contract No. 583/UN26/KU/2017).

REFERENCES

1. Y. Yang, J. You, Make perovskite solar cells stable, Nat. 554, 2017, 155-156.
2. N-G. Park, Perovskite solar cells : an emerging photovoltaic technology, Mat. Today, 18, 2, 2015, 65-72.
3. J.M. Ball, S.D. Stranks, M.T. Horantner, S. Huttner, W. Zhang, E.J.W. Crossland, I. Ramirez, M. Riede, M.B. Johnston, R.H. Friend, H.J. Snaith, Optical properties and limiting photocurrent of thin film perovskite solar cells, Energy Environ. Sci., 8, 2, 2015, 602-609.
4. P.M. Kaminski, P.J.M. Isherwood, G. Womack, J.M. Walls, Optical Optimization of Perovskite Solar Cells Structure for Maximum Current Collection, Energy Proc., 102, 2016, 11-18.
5. A.S. Bhalla, R. Guo, R. Roy, The perovskite structure – a review of its role in ceramic science and technology, Mat. Res. Innov., 4, 1, 2000, 3-26.
6. M.H. Imanieh, H. Rad, A. Nadarajah, J. Gonzalez-Platas, F. Rivera-Lopez, and I.R. Martin, Novel perovskite ceramics for chemical looping combustion

application, J. CO_2 Utilization 13, 2016, 95-104.
7. W. Hortschitz, Steiner H, Stifter M, Kainz A, Kohl F, Siedler C, Schalko J, and Keplinger F, Novel MOEMS Lorentz force transducer for magnetic fields, Proc. Eng., 168, 2016, 680-683.
8. C. Zhang, D. Sun, C-X. Sheng, Y.X. Zhai, K. Mielczarek, A. Zakhidov, Z.V. Vardeny, Magnetic field effects in hybrid perovskite devices, Nat. Phys., 11, 2015, 427-434.
9. J.W. Fergus, Perovskite oxides for semiconductor-based gas sensors, Sens. Act. B: Chem., 123, 2, 2007, 1169-1179.
10. G. Dong, H. Fan, H. Tian, J. Fang, Q. Li, Gas-sensing and electrical properties of perovskite structure p-type barium – substituted bismuth ferrite, RSC Adv., 5(38), 2015, 29618-29623.
11. N. Labhasetwar, G. Saravanan, S. Kumar, M.N. Manwar, R. Khobragade, P. Doggali, F. Grasset, Perovskite – type catalytic materials for environmental applications, Sci. Tech. Adv. Mat., 16, 2015, 036002 , 13 pp.
12. G. Zhang, G. Liu, L. Wang, J.T.S Irvine, Inorganic perovskite photocatalysts for solar energy utilization, Chem. Soc. Rev., 45, 2, 2016, 15951-5984.
13. U. Megha, K. Shijina, G. Varghese, Nanosized $LaCo_{0.6}Fe_{0.4}O_3$ perovskites synthesized by citrate sol gel auto combustion method, Proc. Appl. Ceram., 8, 2, 2014, 87-92.
14. X.C. Liu, R. Hong, C. Tian, Tolerance factor and stability discussion of ABO_3-type ilmenite, J. Mater. Scie. : Mater. Electron., 20, 4, 2009, 323-327.
15. T. Nagai, W. Ito, T. Sakon, Relationship between cation substitution and stability of perovskite structure in $SrCoO_{3-\delta}$-based mixed conductors, Solid Stat. Ion., 177, 2007, 3433-3444.
16. S. Rousseau, S. Loridant, P. Delichere, A. Boreave, J.P. Deloume, P. Vernoux, $La_{(1-x)}Sr_xCo_{(1-y)}Fe_yO_3$ perovskites prepared by sol-gel method : Characterization and relationships with catalytic properties for total oxidation of toluene, Appl. Catal. B: Environ., 88, 2009, 438-447.
17. M. Cernea, F. Vasilliu, C. Plapcianu, C. Bartha, I. Merconiu, I. Pasuk, R. Lowndes, R. Trusca, G.V. Aldica, L. Pintilie, Preparation by sol-gel and solid state reaction methods and properties investigation of double perovskite Sr_2FeMoO_6, J. Eur. Ceram. Soc., 33, 13-14, 2013, 2483-2490.
18. C. Cristiani, G. Dotelli, M. Mariani, R. Pelosato, L. Zampori, Synthesis of nanostructured perovskite powders via simple carbonate co-precipitation, Chem. Papers, 67, 5, 2013, 526-531.
19. E. Mostafavi, A. Babaei, A. Ataie, Synthesis of Nano-structured $La_{0.6}Sr_{0.4}Co_{0.2}Fe_{0.8}O_3$ perovskite by Co-Precipitation Method, J. Ultrafine Grain. nanostructure. Mat., 48, 1, 2015, 45-52.
20. X. Yang, Z. Ren, G. Xu, C. Chao, S. Jiang, S. Deng, G. Shen, X. Wei, G. Han, Monodisperse hollow perovskite BaTiO3 nanostrucutres prepared by a sol gel hydrothermal method, Ceram. Intern., 40, 7, 2014, Part A, 9663-9673.
21. X. Zhang, B. Gao, L. Hu, L. Li, W. Jin, K. Huo, P.K. Chu, Hydrothermal synthesis of provskite-type $MTiO_3$ (M=Zn, Co, Ni)TiO_2 nanotube arrays from an amorphous TiO2 template, Cryst. Eng. Commun., 16, 2014,10280-10285.
22. S. Ueno, K. Nakashima, Y. Sakamoto, S. Wada, Synthesis of Silver-Strontium Titanate Hybrid Nanoparticles by Sol-gel hydrothermal method, Nanomat., 5, 2015, 386-397.
23. S.M. Khetre, H.V. Jadhav, and S.R. Bamane, Synthesis and Characterization of Nanocrystalline $LaFeO_3$ by Combustion Route, Rasayan J. Chem., 3, 1, 2010, 82- 86.
24. J. Vieten, B. Bulfin, M. Lange, M. Schmucker, A. Francke, M. Roeb, C. Sattler, Perovskite oxides for application in thermochemical air separation and oxygen storage, J. Mat. Chem. A., 4, 35, 2016, 13652-13659.
25. F, Deganello, G. Marci, G. Deganello, Citrate-nitrate autocombustion synthesis of perovskite-type nanopowders: A systematic approach, J. Eur. Ceram. Soc., 29, 3, 2009, 439-450.
26. A. Khursheed, M. Akbar, M. Pradeep, M.M. Shaikh, Preparation of SrTiO3 perovskite decorated rGO and electrochemical detection of nitroaromatics, Electrochem. Act., 215, 2016, 435-446.
27. S. Ramesh, Sol-Gel Synthesis and Characterization of $Ag_{3(2+x)}Al_xTi_{4-x}O_{11+\delta}(0.0 \leq x \leq 1.0)$ Nanoparticles, J. Nanosci., 2013, 2013, 929321.
28. R. Situmeang, S. Wibowo, W. Simanjuntak, R. Supryanto, R. Amalia, M. Septanto, P. Manurung, S. Sembiring, Characteristics of nanosize spinel $Ni_xFe_{3-x}O_4$ prepared by sol-gel method using egg white as emulsifying agent. Indones. J. Chem., 15,

2, 2015, 116-122.
29. H. Tavakkoli, D. Beiknejad, T. Tabari, Fabrication of perovskite-type oxide $La_{0.5}Ca_{0.5}CoO_{3-\delta}$ nanoparticles and its Dye removal performance, Desalin. Water Treat., 52, 2014, 37-39.
30. R. Situmeang, R. Supryanto, L.N.A Kahar, W. Simanjuntak, S. Sembiring, Characteristics of Nano-Size $LaCrO_3$ Prepared Through Sol-Gel Route Using Pectin as Emulsifying Agent, Orient. J. Chem., 33, 4, 2017, 1705-1713.
31. B.D. Cullity, Elements of X-ray Diffraction, 2nd ed., Addison-Wesley, 1978, London 102.
32. R. López, R. Gómez, Band-gap energy estimation from diffuse reflectance measurements on sol-gel commercial TiO_2: a Comparative study, J. Sol-Gel Sci. Technol., 61, 1, 2012, 1-7.
33. B. Karvaly, I. Hevesi, Investigations on Diffuse Reflectance Spectra of V_2O_5 Powder, Z. Naturforsch., 26, 11, 1971, 245-249.
34. F. Urbach, The long-wavelength edge of photographic sensitivity and of the electronic absorption of solids, J. Phys. Rev., 92, 5, 1953, 1324.
35. S. Naseem, W. Khan, A.A. Saad, M. Shoeb, H. Ahmed, S. Husain, A.H. Naqvi, Variation in Band Gap of Lanthanum Chromate by Transition Metals Doping $LaCr_{0.9}A_{0.1}O_3$ (A:Fe/Co/Ni), AIP Conf. Proc. 1591, 2014, 259-261.